Applied Materials Today 20 (2020) 100729

Contents lists available at ScienceDirect

Applied Materials Today

journal homepage: www.elsevier.com/locate/apmt

Unraveling how nanoscale curvature drives formation of lysozyme protein monolayers on inorganic oxide surfaces

Abdul Rahim Ferhan[a,1], Bo Kyeong Yoon[b,1], Won-Yong Jeon[b], Joshua A. Jackman[b,*], Nam-Joon Cho[a,*]

[a] School of Materials Science and Engineering, Nanyang Technological University, 50 Nanyang Drive 637553, Singapore
[b] School of Chemical Engineering, Sungkyunkwan University, Suwon 16419, Republic of Korea

ARTICLE INFO

Article history:
Received 26 April 2020
Revised 8 June 2020
Accepted 10 June 2020
Available online xxx

Keywords:
Nanoscale curvature
Protein adsorption
Nanoplasmonic sensing
Localized surface plasmon resonance
Quartz crystal microbalance-dissipation

ABSTRACT

The development of nanostructured material interfaces is critical to various application areas spanning diverse fields such as medicine, energy, and sensing. One of the most promising areas involves nanomedicine and drug delivery and involves the formation of noncovalently adsorbed protein coatings on nanostructured surfaces such as inorganic nanoparticles. The coatings can form naturally as part of the so-called protein corona or be purposely incorporated as functional elements to evade immune recognition or to enable enzymatic function, for example. To date, most relevant studies have examined the underlying adsorption processes on planar surfaces while the effect of nanoscale curvature on protein adsorption is still being unraveled across many dimensions. Herein, we investigated the ionic strength-dependent adsorption of antibacterial lysozyme protein onto planar and nanostructured silicon oxide surfaces by employing the quartz crystal microbalance-dissipation and localized surface plasmon resonance sensing techniques. Our findings revealed that lysozyme undergoes greater adsorption-related denaturation and spreading on planar surfaces which led to multilayer formation, while nanoscale curvature effects suppress protein denaturation on nanostructured surfaces leading to monolayer formation. We discuss these findings within the context of protein-surface and protein-protein interactions and how subtle changes in adsorption pathways can drive the formation of distinct macromolecular assemblies. Looking forward, we also discuss how such measurement strategies can enable mechanistic insights into the formation of protein coatings on nanostructured surfaces with broad implications for nano-bio interface science.

1. Introduction

Nanostructured surfaces are highly relevant to a wide range of material science applications at the nano-bio interface, including tissue engineering [1, 2], biological implant design [3, 4], drug delivery [5, 6], and biosensing [7, 8]. They can offer excellent control over biomacromolecular interactions [9, 10] and can exhibit antimicrobial [11–13] and antifouling [14, 15] properties among various possibilities. With advances in nanofabrication technology, numerous efforts have been made to understand and improve biointerfacial capabilities through a materials engineering approach [16–19]. Within this scope, nanostructured sensor arrays have emerged as a fascinating subset within the broader family of nanostructured surfaces due to their dual functionality as surface-sensitive sensors and topological templates [20–22]. The possibility of replicating biologically relevant nanoscale architectures on these arrays, aided by appropriate surface modification and biological interfacing strategies, facilitates systematic investigations of biointerfacial processes, which would otherwise be impossible or difficult to perform *in vivo*. While earlier works mainly focused on using nanostructured sensor arrays to understand cellular functions and investigate cell-material interactions [23, 24], later studies have been extended towards more deeply exploring the interactions of specific biomacromolecules with nanostructured materials [25–27].

Recent progress in biointerfacial characterization has witnessed the utilization of oxide-coated nanostructured arrays in nanoplasmonic sensing, which is a surface-sensitive measurement technique that is well-suited to monitor biomacromolecular adsorption due to its narrow sensing depth [28, 29]. Nanoplasmonic sensors are typically comprised of an array of noble metal nanostructures that act as optical transducers to detect mass variations close to

* Corresponding author.
E-mail addresses: jjackman@skku.edu (J.A. Jackman), njcho@ntu.edu.sg (N.-J. Cho).
[1] These authors contributed equally to this work.

https://doi.org/10.1016/j.apmt.2020.100729
2352-9407/

their surface based on localized surface plasmon resonance (LSPR) [30–32]. The possibility of introducing a thin conformal layer of a dielectric material over the metallic nanostructure has enabled a wide range of biomacromolecular interaction studies on nanoplasmonic sensing platforms since biologically relevant materials such as silicon oxide, titanium oxide, and aluminum oxide can conformally coat the sensor surface [33]. Besides enabling the direct interaction of biomacromolecules with oxide materials, oxide-coated nanostructured arrays also facilitate biological interfacing [34]. Of note, supported lipid bilayers can be conveniently fabricated on silicon oxide-coated nanoplasmonic sensor arrays for studying various biomacromolecular-membrane interactions [35–38].

To date, a variety of nanoplasmonic sensor arrays have been successfully fabricated with different combinations of nanostructure geometries and oxide coating materials [39–41]. Such developments have initiated a series of systematic studies aimed at understanding the influence of nanoscale lipid membrane geometry on biomacromolecular interactions, including peptide-membrane interactions [42, 43]. In addition, several works have employed nanoplasmonic sensing to study protein adsorption onto inorganic oxide-coated surfaces and scrutinized protein adsorption behavior [41–45]. Interestingly, despite encouraging progress on both of those fronts, the prospect of using oxide-coated nanostructured arrays in nanoplasmonic sensing for the purpose of understanding the effect of nanoscale surface curvature on protein adsorption phenomena remains largely untapped. Unraveling the influence of such curvature on protein adsorption has broad implications across the nano-bio interface field as it can reveal psychochemical insights into foreign body reactions such as corona formation [46–49] and complement activation [50–52] upon the introduction of nanoparticles and biological implants. Research in this direction will ultimately lead to improved biomaterials selection, topographical design, and surface modification that can improve material performance across medical and biotechnology application scopes. So far, protein adsorption works intended at addressing these issues involve colloidal systems (*i.e.*, nanoparticles in solution phase), which offer minimal control [53, 54]. Furthermore, most protein adsorption works typically track the adsorption process at a single length scale and draw conclusions about complex biomacromolecular transformations occurring on the surface [55–57]. In this respect, the possibility of combining nanoplasmonic sensing with a complementary surface-sensitive measurement technique such as quartz crystal microbalance-dissipation (QCM-D) [58, 59] offers the important prospect of deciphering the influence of nanoscale surface curvature on protein adsorption by simultaneously evaluating biomacromolecular interaction processes at nanostructured surfaces with complementary measurement strategies based on different physical principles.

Herein, we employed a silicon oxide-coated gold nanodisk array alongside a flat sensor with the same active surface to compare the adsorption behavior of lysozyme on nanostructured and planar surfaces under various ionic strength conditions. Silicon oxide was selected as the test surface because it is widely used in the biomedical field [60, 61]. Lysozyme was selected as the model protein for several important reasons, apart from its abundance in the physiological system [62]. Firstly, its size (*i.e.*, hydrodynamic diameter of ~4 nm [63]) is well within the effective sensing depth of the nanoplasmonic sensing technique (*i.e.*, ~5-20 nm [64, 65]), ensuring that any molecular structural transformations occurring on the surface can be deduced from the nanoplasmonic signal response. Secondly, lysozyme is known to form multilayers under certain conditions [66, 67], which represents an interesting aspect of protein adsorption that has yet to be fully investigated in relation to surface curvature. Thirdly, the availability of previous experimental [53, 54, 68] and simulation [69, 70] reports on the effect of nanoparticle size, which is often implicitly correlated to the effect of surface curvature, on lysozyme adsorption provides a guiding framework. Finally, it is well-established that lysozyme possesses antimicrobial properties [62, 71] and its potential to form natural antimicrobial coatings are beginning to be explored [72, 73]. In order to monitor lysozyme adsorption process in real-time, we utilized, separately and in tandem, the QCM-D and LSPR techniques. The difference in sensing depths by up to an order of magnitude between these two techniques further enabled us to correlate the conformational changes occurring in the immediate vicinity of the nanostructured and planar surfaces to the overall formation of protein assemblies on the two surfaces.

2. Materials and methods

2.1. Lysozyme preparation

Lyophilized lysozyme from chicken egg white (L6876) was obtained from Sigma-Aldrich (Singapore) and was stored at 4°C prior to use. Buffer solutions were prepared using 10 mM Tris(hydroxymethyl)aminomethane (Tris) and varying concentrations of sodium chloride (Sigma-Aldrich, Singapore). All buffer solutions were adjusted to pH 7.5 with 1 M hydrochloric acid (Sigma-Aldrich, Singapore), and filtered through a membrane filter with 0.22 μm diameter pores before use. All protein samples were freshly prepared on the day of experiments by dissolving a weighed mass of lyophilized protein in the appropriate buffer solution.

2.2. QCM-D measurements

QCM-D measurements were performed on a Q-Sense E4 instrument (Biolin Scientific AB, Gothenburg, Sweden) using AT-cut crystals with a sputter-coated, 50 nm-thick silicon oxide layer (QSX 303, Biolin Scientific), as previously described [58]. The crystals had a mass sensitivity constant of 17.7 ng/cm^2 Hz. Before measurement, the crystals were rinsed with 1 wt% SDS in water, water, and ethanol, dried with a stream of nitrogen gas, and treated with oxygen plasma for 1 min (Harrick Plasma). Samples were introduced at a constant flow rate of 100 µL/min, as regulated by a peristaltic pump (Reglo Digital), and the temperature of the measurement cell was maintained at 25.0 ± 0.5°C. Data was collected at the odd overtones (3rd, 5th, 7th, and 9th), and normalized data at the 5th overtone are reported.

2.3. LSPR measurements

Ensemble-averaged LSPR measurements were performed on an Insplorion XNano instrument (Insplorion AB, Gothenburg, Sweden) that was operated in transmission mode, as previously described [58]. The sensor chips were composed of silicon oxide-coated gold nanodisk arrays on glass surfaces, which were assembled within the measurement cell. The arrays are comprised of well-separated and randomly distributed gold nanodisks (average height and diameter of 20 and 120 nm, respectively, with a surface coverage of ~8%), which were fabricated by hole-mask lithography, and sputter-coated with a thin silicon nitride layer (thickness ~10 nm). Prior to each experiment, the sensor chips were thoroughly rinsed with 1 wt% sodium dodecyl sulfate (SDS) in water, water, and ethanol and dried with a stream of nitrogen gas. The sensor chips were then treated with oxygen plasma (Harrick Plasma, Ithaca, NY), converting the uppermost region of the silicon nitride layer into a silicon oxide coating and then the sensor chip was loaded into the measurement cell. A peristaltic pump (Reglo Digital, Ismatec, Glattbrugg, Switzerland) was used to introduce liquid sample into the measurement cell at a constant flow rate of 100 µL/min. All LSPR data collection and analysis was performed using the Insplorer

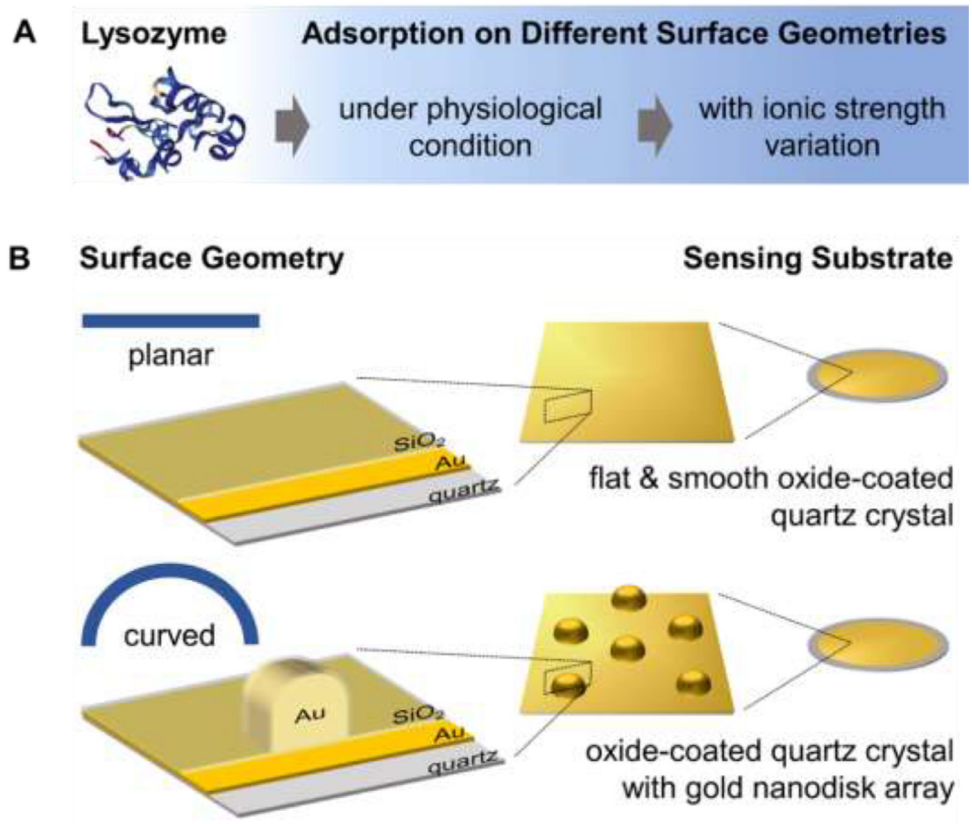

Fig. 1. (A) Schematic illustration of the overall experimental strategy. (B) QCM-D sensing substrate architectures employed in this work to model planar and nanostructured surfaces.

software package (Insplorion AB) with a time resolution of 1 Hz. The spectral resolution of the plasmon resonance as well as its centroid position (denoted as λ_{max}) was determined by high-order polynomial fitting.

2.4. Combined QCM-D and LSPR measurements

The combined QCM-D and LSPR setup is comprised of the Q-Sense E1 system with Q-Sense QWM401 window module (Biolin Scientific, Stockholm, Sweden) together with the Insplorion Acoulyte module (Insplorion AB, Gothenburg, Sweden), which provides an optical connection between the QCM-D measurement chamber and the Insplorion X-Nano optics unit (Insplorion AB, Gothenburg, Sweden). Measurements were performed on the Acoulyte quartz crystal sensor, which is a modified version of a typical QCM-D sensor chip upon which randomly distributed, silicon oxide-coated gold nanodisks were fabricated, as previously described [58].

3. Results and discussion

3.1. Measurement strategy

In order to understand the adsorption behavior of lysozyme on silicon oxide surfaces with different geometries in a comprehensive manner, the adsorption experiments were conducted under varying ionic strength conditions (Fig. 1A). As a point of reference for adsorption on a planar geometry, the measurements were first performed on the conventional QCM-D platform using standard quartz crystal sensors with a flat and smooth silicon oxide surface (Fig. 1B). The adsorption on nanostructured geometry was then performed on silicon oxide-coated gold nanodisk arrays using the conventional LSPR platform as well as using a combined QCM-D and LSPR platform. In the conventional LSPR platform, the gold nanodisks were fabricated on a transparent glass support substrate. The sensor architecture is slightly modified in the combined QCM-D and LSPR platform, whereby the gold nanodisks were fabricated on top of the QCM-D quartz crystal sensor chip. In both cases, apart from acting as a curvature template, the gold nanodisks serve as optical transducers. Upon interaction with light, a collective oscillation of free electrons is generated in the metal conduction band, which is known as localized surface plasmon resonance (LSPR) [74]. This enhances the evanescent electromagnetic field near the surface of the nanostructures. At the same time, it leads to light extinction over the UV-visible range with a maximum at a specific wavelength, λ_{max}, which is sensitive to the local dielectric environment [75, 76]. During LSPR measurements, the accumulation of mass near the surface leads to an LSPR peak shift, $\Delta\lambda_{max}$, which can be correlated to the amount of adsorbed lysozyme as well as the degree of surface-induced protein denaturation. In the combined QCM-D and LSPR platform, the QCM-D frequency and dissipation shifts were extracted simultaneously together with the LSPR peak shifts. Since the sensing depths of the QCM-D and LSPR techniques are around 100-200 nm [77] and 5-20 nm [64, 65], respectively, the use of these two techniques is therefore beneficial to resolve differences in the state of adsorbed proteins across different length scales.

3.2. QCM-D evaluation of concentration-dependent adsorption behavior on planar surfaces

Protein adsorption measurements were performed in a continuous flow-through environment and the measurement signals were recorded in real-time. Briefly, the measurement baseline was first obtained in a blank buffer before introducing the lysozyme sample

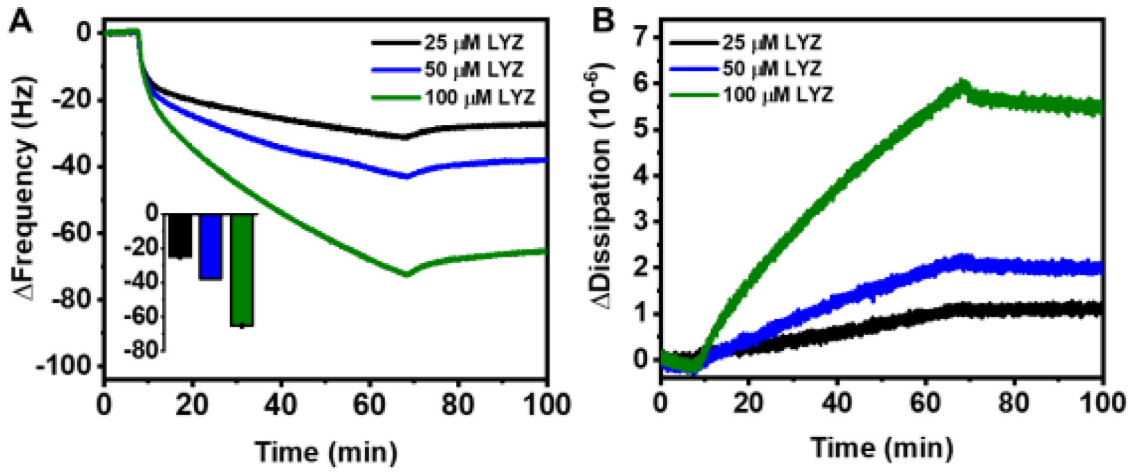

Fig. 2. Time-resolved QCM-D (A) frequency and (B) dissipation shifts following the lysozyme adsorption onto the silicon oxide-coated planar substrate at different protein concentrations. The measurement baseline signal was first obtained in blank buffer followed by the injection of lysozyme in buffer at around 10 min and a final washing step at around 70 min. Inset in panel (A) shows mean ± standard deviation of maximum frequency shifts from n=4 measurements.

in buffer solution. The adsorption process continued until reaching pseudo-steady-state, after which the system underwent a buffer washing step. Time-resolved measurements obtained using standard silicon oxide-coated QCM-D quartz crystal sensor chips with a flat surface under physiologically relevant conditions revealed that the QCM-D frequency shifts increased at higher lysozyme concentration, indicating greater overall mass adsorbed on the surface at higher protein concentrations (Fig. 2A). The frequency shifts in the pseudo-steady-state adsorption regime as well as after buffer washing were relatively proportional to the lysozyme concentration in the buffer solution, suggesting that adsorption within this concentration range did not lead to saturation uptake. However, since QCM-D has a relatively lower surface sensitivity than LSPR, this finding implies that the concentration range is either too low to saturate the surface, or that it leads to the formation of lysozyme multilayers. In order to distinguish between these possibilities, we analyzed the QCM-D dissipation shifts, which provide an indication of viscoelasticity of the adsorbed layer. Lower dissipation shifts are generally associated with protein layers that are tightly bound to the surface, while higher dissipation shifts are associated with less rigid layers. The results showed that the QCM dissipation shifts increase with lysozyme concentration (Fig. 2B). In other words, lysozyme adsorbed into a rigid adlayer at a low concentration. With increasing concentration, the overall protein ensemble gradually became less rigid, supporting the formation of lysozyme multilayers.

3.3. QCM-D evaluation of ionic strength-dependent adsorption behavior on planar surfaces

We then performed subsequent measurements at an intermediate protein concentration of 50 μM to determine the ionic strength dependency of the protein adsorption process. The influence of ionic strength is often associated with the electrostatic modulation of protein-substrate and protein-protein interactions and ionic strength variation can therefore serve as a means to understand the role of these interactions within the adsorption process [45, 78, 79]. In this work, ionic strength variation was achieved by adjusting the NaCl concentration in the buffer solution. We found that the frequency shift in the pseudo-steady-state adsorption regime and after buffer washing increased when the NaCl concentration was raised from 50 mM to 150 mM while tending to slightly decrease at 250 mM (Fig. 3A). It is noteworthy that the adsorption kinetics in 50 mM NaCl varied modestly from those observed in 150 mM and 250 mM NaCl. In 50 mM NaCl, the initial rate of adsorption was very high, followed by a gradual stabilization suggesting that there were strong protein-surface interactions leading to rapid adsorption with minimal protein denaturation [80, 81], which subsequently hampers multilayer formation. An opposite trend was observed at higher ionic strengths, whereby the initial adsorption rate is lower but the rates in the pseudo-steady-state regime are higher than at 50 mM NaCl, implying an increased tendency of multilayer formation. Despite the non-monotonic trend observed in the pseudo-steady-state regime, which arises from the propensity to form a monolayer at 50 mM NaCl and multilayers at 150 mM and 250 mM NaCl, there is a consistent decrease in the initial adsorption rate with increasing ionic strength, which agrees well with previous works [81-85]. The decrease in initial rates is attributed to a charge shielding effect which reduces the protein-surface interaction between positively charged lysozyme molecules and the negatively charged silicon oxide surface in the presence of salt. Similarly, the dissipation shift increased when the ionic strength was raised from 50 mM to 150 mM NaCl (Fig. 3B). Although the dissipation shift further decreased slightly from 150 mM to 250 mM NaCl, it remained significantly higher compared to the 50 mM NaCl condition and the trend in dissipation shifts agreed well with the overall amount of adsorbed proteins on the surface across all tested ionic strength conditions. Importantly, the high dissipation values observed in 150 mM and 250 mM NaCl reflected the tendency for multilayer formation while the low dissipation value observed in 50 mM NaCl was consistent with monolayer formation. Taken together, our results suggest that, on planar geometries, the assembly of adsorbed lysozyme molecules can be modulated between monolayer and multilayer configurations by adjusting the ionic strength of the solution.

3.4. LSPR evaluation of ionic strength-dependent adsorption behavior on nanostructured surfaces

In order to determine whether the assembly of lysozyme on a nanostructured surface can be similarly modulated via ionic strength, we proceeded to investigate the ionic strength dependency of lysozyme adsorption behavior onto a silicon oxide-coated gold nanodisk sensor array via LSPR measurements. Over the same range of ionic strength conditions, the observed trend varied significantly from the QCM-D results. Time-resolved measurements revealed an overall consistent decrease in LSPR peak shift, $\Delta\lambda_{max}$, with increasing ionic strength (Fig. 4A). Since LSPR is a highly

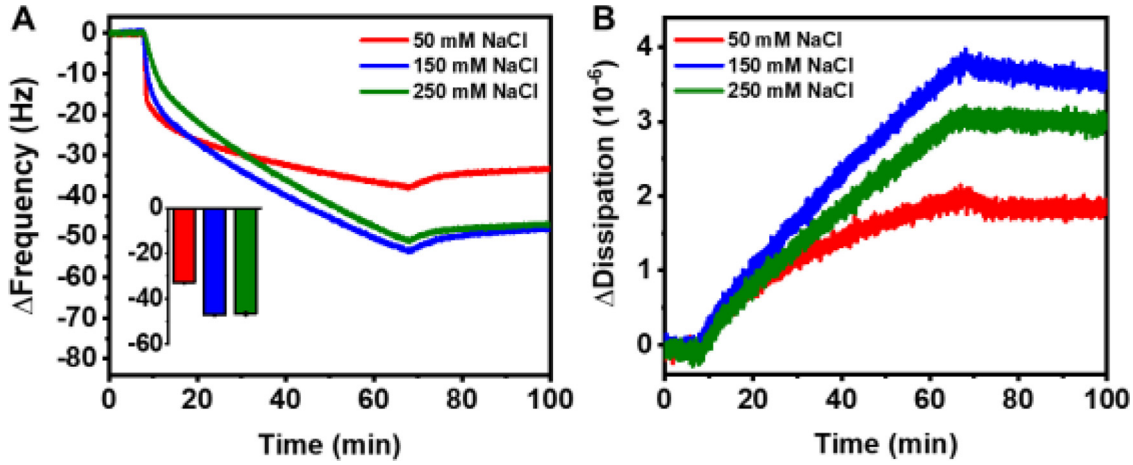

Fig. 3. Time-resolved QCM-D (A) frequency and (B) dissipation shifts following the lysozyme adsorption onto a silicon oxide-coated planar substrate under different ionic strength conditions, as modulated by NaCl concentration. The measurement baseline signal was first obtained in blank buffer followed by the injection of lysozyme in buffer at around 10 min and a final washing step at around 70 min. Inset in panel (A) shows mean ± standard deviation of maximum frequency shifts from n=4 measurements.

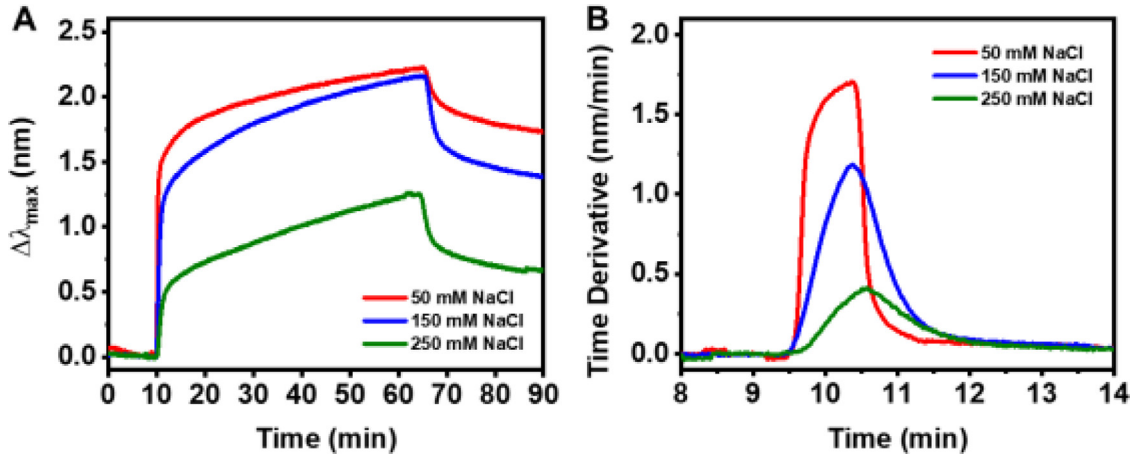

Fig. 4. Time-resolved LSPR (A) peak shifts, $\Delta\lambda_{max}$, and (B) corresponding time derivatives, $d(\Delta\lambda_{max})/dt$, following lysozyme adsorption onto a silicon oxide-coated gold nanodisk array under different ionic strength conditions, as modulated by NaCl concentration. The measurement baseline signal was first obtained in blank buffer followed by the injection of lysozyme in buffer at around 10 min and a final washing step at around 70 min.

surface-sensitive technique that detects only protein mass in the immediate vicinity of the sensing surface, the results suggest that there is less lysozyme adsorption at higher ionic strength, which agrees well with previous works that cite charge shielding effects as the primary reason behind this trend [82, 83]. We then calculated the time derivative of the peak shift, $d(\Delta\lambda_{max})/dt$, to observe the initial rate of protein adsorption. The initial rate of adsorption decreased monotonically with increasing ionic strength (Fig. 4B). Interestingly, this result is consistent with the trend observed for the rate of initial lysozyme adsorption onto the planar surface in the QCM-D measurements. In other words, the initial adsorption behavior is similar on both planar and nanostructured surfaces since it is governed by the same protein-surface interactions. However, the later stage of adsorption appears to differ significantly, and the data suggests that while multilayer formation is supported on planar surfaces, it is suppressed on nanostructured surfaces.

3.5. Simultaneous QCM-D and LSPR measurements on nanostructured surfaces

We also conducted equivalent measurements under physiological (150 mM NaCl) and elevated (250 mM NaCl) ionic strength conditions on the combined QCM-D and LSPR platform using the modified quartz crystal sensor chip comprising a silicon oxide-coated gold nanodisk array. The ionic strength conditions were selected because we observed possible multilayer formation on the planar surface in the QCM-D measurements. By comparing those results with the QCM-D response signal from the combined platform, which presents a nanostructured surface, it is thus possible to differentiate between the adsorption behavior on both surface geometries. At the same time, it is also possible to extract the LSPR signals to gain insight into lysozyme adsorption behavior at different length scales above the sensor surface. Indeed, the trend observed for the frequency shifts obtained from the combined QCM-D and LSPR platform experiments (Fig. 5A) differs from that observed on the conventional QCM-D platform, whereas it resembles the trend obtained from the conventional LSPR measurements (*cf.* Fig. 4A). This finding supports that the difference in adsorption trends arises from the different surface geometries (*i.e.*, planar or nanostructured). The stabilized frequency shifts under both ionic strength conditions were also much lower than those on the conventional QCM-D system, indicating less adsorption uptake on the nanostructured surface as opposed to on the planar surface.

Interestingly, the dissipation shifts were not only smaller, but remained relatively unchanged under both ionic strength conditions with values less than 1.0×10^{-6} (Fig. 5B). This finding suggests that lysozyme adsorbs tightly on the nanostructured surface to form a monolayer and the difference in adsorbed mass

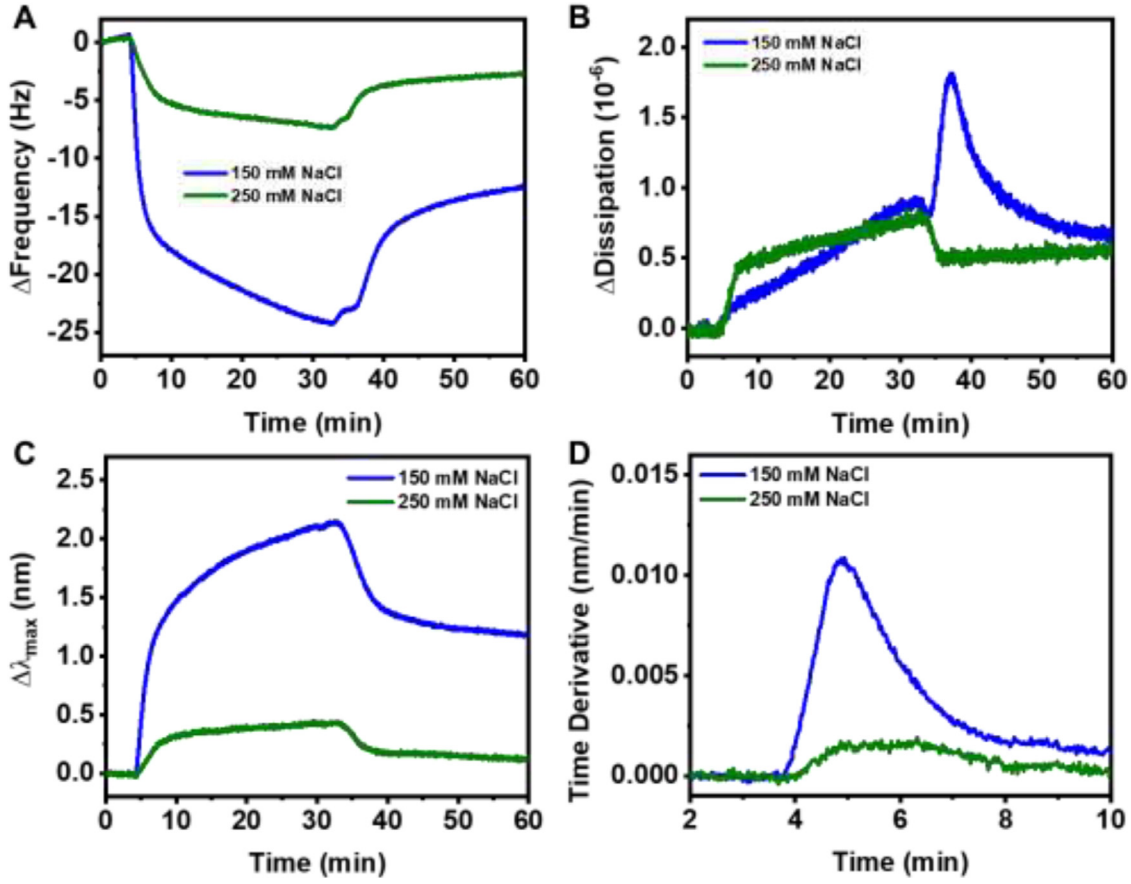

Fig. 5. Time-resolved QCM-D (A) frequency and (B) dissipation shifts, and simultaneously recorded (C) LSPR peak shifts, $\Delta\lambda_{max}$, and corresponding (D) time derivatives, $d(\Delta\lambda_{max})/dt$, for lysozyme adsorption onto a silicon oxide-coated gold nanodisk array under different ionic strength conditions, as modulated by NaCl concentration. The measurement baseline signal was first obtained in blank buffer followed by the injection of lysozyme in buffer at around 5 min and a final washing step at around 35 min.

arises from changes in protein density within the monolayer instead of a transition from monolayer to multilayer. Further time-independent analysis showed that the overall adsorption behavior is similar across different ionic strength conditions on planar surfaces but differs on nanostructured surfaces within this ionic strength regime (**Supplementary Fig. 1**). This result indicates that the effect of charge shielding is greater on nanostructured surfaces, implying that protein-surface interactions influence adsorption behavior to a greater extent in that case. The LSPR peak shifts extracted from the combined platform verified the trend observed on the conventional LSPR platform (Fig. 5C). Likewise, the corresponding time derivatives also confirmed that the initial rate of adsorption decreases with increasing ionic strength (Fig. 5D).

3.6. Comparison of lysozyme adsorption on planar and nanostructured surfaces

On the planar surface and under physiological ionic strength conditions, the stabilized absolute QCM-D frequency shifts before and after washing were around 55 Hz and 48 Hz, respectively (Fig. 6A). On the nanostructured surface, the corresponding values were considerably lower at around 25 Hz and 12 Hz before and after washing, respectively. It is noteworthy that increasing the ionic strength (*i.e.*, to 250 mM NaCl) did not lead to a significant change in absolute frequency shifts on the planar surface but led to a significant decrease on the nanostructured surface (Fig. 6B). The corresponding dissipation shifts on the planar surface and under physiological ionic strength conditions before and after washing were around 3.7×10^{-6} and 3.6×10^{-6}, respectively (Fig. 6C). On the nanostructured surface, the respective values were around 0.8×10^{-6} and 0.6×10^{-6}. Under elevated ionic strength conditions, the dissipation shifts on the planar surface were slightly lower than observed under physiological ionic strength conditions, despite similar frequency shifts observed under both ionic strength conditions (Fig. 6D). Conversely, on the nanostructured surface, the dissipation shifts remained relatively unchanged when the ionic strength was elevated. Taken together, these findings support that lysozyme forms a more discrete assembly on the nanostructured surface. Furthermore, the assembly on the nanostructured surface is more strongly influenced by ionic strength than on planar surfaces.

Based on multiples lines of evidence obtained using the flat sensor and nanostructured array, we conclude that while the initial adsorption behavior of lysozyme on planar and nanostructured silicon oxide surfaces followed the same trends, later stages of adsorption showed significant differences. These variations relate to different degrees of surface-induced protein denaturation on the two surfaces, as illustrated in Fig. 7.

On the planar surface, lysozyme molecules undergo greater surface-induced denaturation since more contacts points can be established between proteins and the surface through van der Waals interactions via specific protein residues. In addition, the thin hydration layer on a planar surface can be easily displaced in the presence of strong protein-surface interactions [55, 86]. This results in greater protein spreading, which leads to the formation of a thin first layer of lysozyme on the surface. The significant degree of protein conformational changes also leads to charge redistribution within this layer, which reduces charge repulsion be-

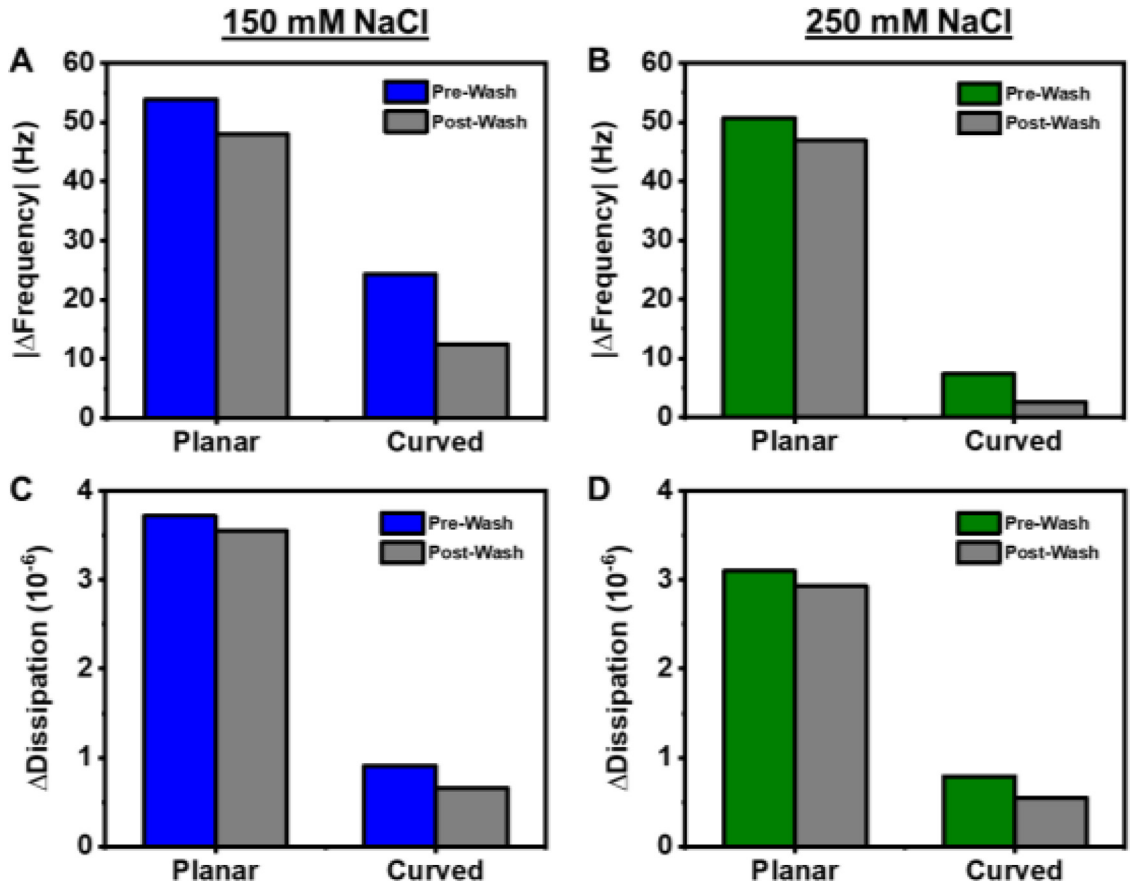

Fig. 6. Comparison of QCM-D final frequency shifts arising from the adsorption of lysozyme on planar and nanostructured silicon oxide-coated substrates in (A) 150 mM and (B) 250 mM NaCl. Corresponding QCM-D final dissipation shifts in (C) 150 mM and (D) 250 mM NaCl.

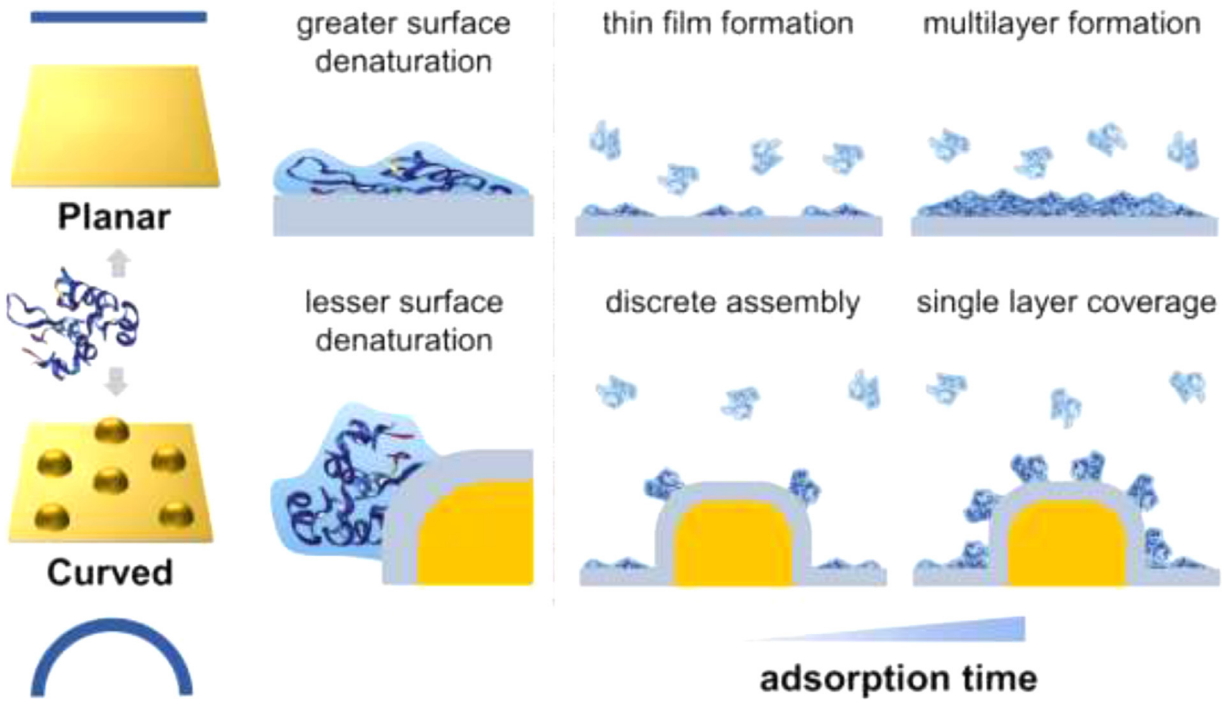

Fig. 7. Summary of lysozyme protein adsorption behavior on planar versus nanostructured silicon oxide surfaces based on the findings in this study.

tween adsorbed and incoming protein molecules from the solution phase [68, 87]. This facilitates the formation of multilayers in the second stage of the adsorption process through van der Waals interactions. By contrast, on the nanostructured surface, lysozyme experiences less surface-induced denaturation since fewer contact points can be established between proteins and the surface. This agrees well with past observations by Vertegel *et al.* on silicon oxide nanoparticles of different sizes [53]. The thin hydration layer on a nanostructured surface is also more tightly bound and difficult to be displaced [69, 88, 89]. With less extensive denaturation, the conformation of adsorbed lysozyme molecules is somewhat preserved in this case. This, in turn, introduces steric hindrance to adsorbing protein molecules from the solution. Taken together, these factors lead to a similar adsorption profile between planar and nanostructured surface in the initial adsorption stage, while the multilayer formation observed in the second stage of lysozyme adsorption onto the planar surface is prevented on the nanostructured surface. Hence, adsorption on the nanostructured surface leads to formation of a single monolayer of lysozyme. These variations in protein assembly also contribute to striking differences in ionic strength dependencies of the adsorption process on the two surfaces. Since the formation of multilayers in the second stage of protein adsorption on the planar surface is mainly driven by van der Waals interactions, it is not governed by electrostatic interactions and the overall adsorption process is therefore not strongly influenced by ionic strength. This contrasts with protein adsorption on the nanostructured surface, which is predominantly electrostatically-driven due to interactions between the positively charged native lysozyme in solution and negatively charged silicon oxide surface. The overall adsorption process on the nanostructured surface is therefore more affected by ionic strength modulation, demonstrating the utility of controlling both the nanotopography of a material surface and environmental conditions in order to fabricate nano-bio interfaces with desired properties.

4. Conclusions

We have systematically investigated the effect of nanoscale surface curvature on lysozyme protein adsorption behavior across flat and nanostructured silicon oxide surfaces and discovered key differences in how protein-substrate and protein-protein interactions drive the formation of adsorbed protein layers on the two surface geometries, akin to protein corona assembly in natural biological systems. Experimentally, we first tracked the adsorption process under a wide range of ionic strength conditions using the QCM-D and LSPR techniques separately, before conducting selected measurements on a combined QCM-D and LSPR platform in order to unravel nanoscale curvature effects. The difference in effective sensing depths between these two techniques enabled us to resolve the adsorption process across different length scales and correlate the conformational changes occurring in the immediate vicinity of the surface to the overall protein assembly. Our results revealed significant variation in the adsorption behavior of lysozyme on planar and nanostructured surfaces. Of note, while the formation of a lysozyme multilayer was observable on planar surfaces, it was not evident on nanostructured surfaces. This is attributed to greater surface-induced protein denaturation and protein spreading on the planar surface, resulting in the formation of a thin protein adlayer, which permits the accumulation of subsequent protein adlayers. By contrast, less favorable protein-surface interactions on a nanostructured surface results in a lower degree of protein spreading, which prevents multilayer formation. The difference in protein assembly arising from varying protein-surface interactions also contribute to striking differences in ionic strength dependencies of the adsorption process on the two surfaces. Taken together, the experimental framework developed in this work can be adopted for the utilization of nanostructured sensor arrays to unravel curvature effects on the adsorption behavior of other proteins beyond lysozyme as well. More importantly, our results highlight the vast potential of surfaces with engineered nanostructures to decipher a broad range of biointerfacial processes and hold broad relevance for exploring nano-bio application topics such as protein corona formation.

Declaration of Competing Interests

The authors declare that they have no known competing financial interests or personal relationships that could have appeared to influence the work reported in this paper.

CRediT authorship contribution statement

Abdul Rahim Ferhan: Conceptualization, Investigation, Writing - original draft, Writing - review & editing. **Bo Kyeong Yoon:** Conceptualization, Investigation, Writing - review & editing. **Won-Yong Jeon:** Investigation, Writing - review & editing. **Joshua A. Jackman:** Conceptualization, Writing - original draft, Writing - review & editing, Supervision. **Nam-Joon Cho:** Conceptualization, Writing - review & editing, Supervision.

Data availability

The raw data required to reproduce these findings are available from the corresponding authors on reasonable request.

Acknowledgements

This work was supported by National Research Foundation of Korea (NRF) grants funded by the Korean government (MSIT) (No. 2020R1C1C1004385 and No. 2020R1C1C1005523). In addition, this work was supported by the Korea Research Fellowship Program through the National Research Foundation of Korea (NRF) funded by the Ministry of Science and ICT (2019H1D3A1A01070318).

Supplementary materials

Supplementary material associated with this article can be found, in the online version, at doi:10.1016/j.apmt.2020.100729.

References

[1] T. Dvir, B.P. Timko, D.S. Kohane, R. Langer, Nanotechnological strategies for engineering complex tissues, Nat. Nanotechnol. 6 (2011) 13–22.
[2] X. Li, L. Wang, Y. Fan, Q. Feng, F.Z. Cui, F. Watari, Nanostructured scaffolds for bone tissue engineering, J. Biomed. Mater. Res., Part A 101 (2013) 2424–2435.
[3] R. Rasouli, A. Barhoum, H. Uludag, A review of nanostructured surfaces and materials for dental implants: surface coating, patterning and functionalization for improved performance, Biomater. Sci. 6 (2018) 1312–1338.
[4] F. Variola, J.B. Brunski, G. Orsini, P. Tambasco de Oliveira, R. Wazen, A. Nanci, Nanoscale surface modifications of medically relevant metals: state-of-the art and perspectives, Nanoscale 3 (2011) 335–353.
[5] T. Lebold, C. Jung, J. Michaelis, C. Bräuchle, Nanostructured silica materials as drug-delivery systems for Doxorubicin: single molecule and cellular studies, Nano Lett 9 (2009) 2877–2883.
[6] M. Goldberg, R. Langer, X. Jia, Nanostructured materials for applications in drug delivery and tissue engineering, J. Biomater. Sci. Polym. Ed. 18 (2007) 241–268.
[7] B. Xiao, S.K. Pradhan, K.C. Santiago, G.N. Rutherford, A.K. Pradhan, Topographically engineered large scale nanostructures for plasmonic biosensing, Sci. Rep. 6 (2016) 24385.
[8] N. Wongkaew, M. Simsek, C. Griesche, A.J. Baeumner, Functional nanomaterials and nanostructures enhancing electrochemical biosensors and lab-on-a-chip performances: recent progress, applications, and future perspective, Chem. Rev. 119 (2019) 120–194.
[9] T. Shibata, Y. Fujita, H. Ohno, Y. Suzuki, K. Hayashi, K.R. Komatsu, S. Kawasaki, K. Hidaka, S. Yonehara, H. Sugiyama, M. Endo, H. Saito, Protein-driven RNA nanostructured devices that function in vitro and control mammalian cell fate, Nat. Commun. 8 (2017) 540.

[10] M. Shiozawa, H. Takeuchi, Y. Akiba, K. Eguchi, N. Akiba, Y. Aoyagi, M. Nagasawa, H. Kuwae, K. Izumi, K. Uoshima, J. Mizuno, Biological reaction control using topography regulation of nanostructured titanium, Sci. Rep. 10 (2020) 2438.
[11] B. Li, X. Xia, M. Guo, Y. Jiang, Y. Li, Z. Zhang, S. Liu, H. Li, C. Liang, H. Wang, Biological and antibacterial properties of the micro-nanostructured hydroxyapatite/chitosan coating on titanium, Sci. Rep. 9 (2019) 14052.
[12] A. Baranwal, A. Srivastava, P. Kumar, V.K. Bajpai, P.K. Maurya, P. Chandra, Prospects of nanostructure materials and their composites as antimicrobial agents, Front. Microbiol. 9 (2018) 422.
[13] G. Benetti, E. Cavaliere, F. Banfi, L. Gavioli, Antimicrobial nanostructured coatings: a gas phase deposition and magnetron sputtering perspective, Materials 13 (2020) 784.
[14] P. Sathe, K. Laxman, M.T.Z. Myint, S. Dobretsov, J. Richter, J. Dutta, Bioinspired nanocoatings for biofouling prevention by photocatalytic redox reactions, Sci. Rep. 7 (2017) 3624.
[15] M.S. Selim, S.A. El-Safty, M.A. Shenashen, S.A. Higazy, A. Elmarakbi, Progress in biomimetic leverages for marine antifouling using nanocomposite coatings, J. Mater. Chem. B 8 (2020) 3701–3732.
[16] S.G. Higgins, M. Becce, A. Belessiotis-Richards, H. Seong, J.E. Sero, M.M. Stevens, High-aspect-ratio nanostructured surfaces as biological metamaterials, Adv. Mater. 32 (2020) 1903862.
[17] L. Hanson, W. Zhao, H.-Y. Lou, Z.C. Lin, S.W. Lee, P. Chowdary, Y. Cui, B. Cui, Vertical nanopillars for in situ probing of nuclear mechanics in adherent cells, Nat. Nanotechnol. 10 (2015) 554–562.
[18] M.J. Dalby, N. Gadegaard, R.O.C. Oreffo, Harnessing nanotopography and integrin–matrix interactions to influence stem cell fate, Nat. Mater. 13 (2014) 558–569.
[19] M.M. Stevens, J.H. George, Exploring and engineering the cell surface interface, Science 310 (2005) 1135.
[20] R.A. Potyrailo, R.K. Bonam, J.G. Hartley, T.A. Starkey, P. Vukusic, M. Vasudev, T. Bunning, R.R. Naik, Z. Tang, M.A. Palacios, M. Larsen, L.A. Le Tarte, J.C. Grande, S. Zhong, T. Deng, Towards outperforming conventional sensor arrays with fabricated individual photonic vapour sensors inspired by Morpho butterflies, Nat. Commun. 6 (2015) 7959.
[21] W. Wang, L. Qi, Light management with patterned micro- and nanostructure arrays for photocatalysis, photovoltaics, and optoelectronic and optical devices, Adv. Funct. Mater. 29 (2019) 1807275.
[22] S. Roy, Z. Gao, Nanostructure-based electrical biosensors, Nano Today 4 (2009) 318–334.
[23] J. Zhou, X. Zhang, J. Sun, Z. Dang, J. Li, X. Li, T. Chen, The effects of surface topography of nanostructure arrays on cell adhesion, Phys. Chem. Chem. Phys. 20 (2018) 22946–22951.
[24] R. Wierzbicki, C. Køber, M.R.B. Jensen, J. Łopacińska, M.S. Schmidt, M. Skolimowski, F. Abeille, K. Qvortrup, K. Mølhave, Mapping the complex morphology of cell interactions with nanowire substrates using FIB-SEM, PLOS ONE 8 (2013) e53307.
[25] T. Lee, J.-S. Wi, A. Oh, H.-K. Na, J. Lee, K. Lee, T.G. Lee, S. Haam, Highly robust, uniform and ultra-sensitive surface-enhanced Raman scattering substrates for microRNA detection fabricated by using silver nanostructures grown in gold nanobowls, Nanoscale 10 (2018) 3680–3687.
[26] T. Lee, S. Kwon, S. Jung, H. Lim, J.-J. Lee, Macroscopic Ag nanostructure array patterns with high-density hotspots for reliable and ultra-sensitive SERS substrates, Nano Res 12 (2019) 2554–2558.
[27] D. Garoli, H. Yamazaki, N. Maccaferri, M. Wanunu, Plasmonic nanopores for single-molecule detection and manipulation: toward sequencing applications, Nano Lett 19 (2019) 7553–7562.
[28] J.A. Jackman, A.R. Ferhan, N.-J. Cho, Nanoplasmonic sensors for biointerfacial science, Chem. Soc. Rev. 46 (2017) 3615–3660.
[29] B. Špačková, N.S. Lynn, J. Slabý, H. Šípová, J. Homola, A route to superior performance of a nanoplasmonic biosensor: consideration of both photonic and mass transport aspects, ACS Photonics 5 (2018) 1019–1025.
[30] V. Giannini, A.I. Fernández-Domínguez, S.C. Heck, S.A. Maier, Plasmonic nanoantennas: fundamentals and their use in controlling the radiative properties of nanoemitters, Chem. Rev. 111 (2011) 3888–3912.
[31] H. Xin, B. Namgung, L.P. Lee, Nanoplasmonic optical antennas for life sciences and medicine, Nat. Rev. Mater. 3 (2018) 228–243.
[32] W. Li, L. Zhang, J. Zhou, H. Wu, Well-designed metal nanostructured arrays for label-free plasmonic biosensing, J. Mater. Chem. C 3 (2015) 6479–6492.
[33] C. Langhammer, E.M. Larsson, B. Kasemo, I. Zorić, Indirect nanoplasmonic sensing: ultrasensitive experimental platform for nanomaterials science and optical nanocalorimetry, Nano Lett. 10 (2010) 3529–3538.
[34] S.-H. Oh, H. Altug, Performance metrics and enabling technologies for nanoplasmonic biosensors, Nat. Commun. 9 (2018) 5263.
[35] A.R. Ferhan, B.K. Yoon, S. Park, T.N. Sut, H. Chin, J.H. Park, J.A. Jackman, N.-J. Cho, Solvent-assisted preparation of supported lipid bilayers, Nat. Protoc. 14 (2019) 2091–2118.
[36] M.P. Jonsson, P. Jönsson, A.B. Dahlin, F. Höök, Supported lipid bilayer formation and lipid-membrane-mediated biorecognition reactions studied with a new nanoplasmonic sensor template, Nano Lett. 7 (2007) 3462–3468.
[37] A. Dahlin, M. Zäch, T. Rindzevicius, M. Käll, D.S. Sutherland, F. Höök, Localized surface plasmon resonance sensing of lipid-membrane-mediated biorecognition events, J. Am. Chem. Soc. 127 (2005) 5043–5048.
[38] J.A. Jackman, N.-J. Cho, Supported lipid bilayer formation: beyond vesicle fusion, Langmuir 36 (2020) 1387–1400.
[39] F.A.A. Nugroho, D. Albinsson, T.J. Antosiewicz, C. Langhammer, Plasmonic metasurface for spatially resolved optical sensing in three dimensions, ACS Nano 14 (2020) 2345–2353.
[40] F.A.A. Nugroho, R. Frost, T.J. Antosiewicz, J. Fritzsche, E.M. Larsson Langhammer, C. Langhammer, Topographically flat nanoplasmonic sensor chips for biosensing and materials science, ACS Sens 2 (2017) 119–127.
[41] C. Zhao, X. Xu, A.R. Ferhan, N. Chiang, J.A. Jackman, Q. Yang, W. Liu, A.M. Andrews, N.-J. Cho, P.S. Weiss, Scalable fabrication of Quasi-one-dimensional gold nanoribbons for plasmonic sensing, Nano Lett. 20 (2020) 1747–1754.
[42] G. Emilsson, E. Röder, B. Malekian, K. Xiong, J. Manzi, F.-C. Tsai, N.-J. Cho, M. Bally, A. Dahlin, Nanoplasmonic sensor detects preferential binding of IRSp53 to negative membrane curvature, Front. Chem. 7 (2019).
[43] A.R. Ferhan, J.A. Jackman, B. Malekian, K. Xiong, G. Emilsson, S. Park, A.B. Dahlin, N.-J. Cho, Nanoplasmonic sensing architectures for decoding membrane curvature-dependent biomacromolecular interactions, Anal. Chem. 90 (2018) 7458–7466.
[44] J.A. Jackman, A.R. Ferhan, B.K. Yoon, J.H. Park, V.P. Zhdanov, N.-J. Cho, Indirect nanoplasmonic sensing platform for monitoring temperature-dependent protein adsorption, Anal. Chem. 89 (2017) 12976–12983.
[45] A.R. Ferhan, J.A. Jackman, T.N. Sut, N.-J. Cho, Quantitative comparison of protein adsorption and conformational changes on dielectric-coated nanoplasmonic sensing arrays, Sensors 18 (2018) 1283.
[46] P.d. Pino, B. Pelaz, Q. Zhang, P. Maffre, G.U. Nienhaus, W.J. Parak, Protein corona formation around nanoparticles – from the past to the future, Mater. Horiz. 1 (2014) 301–313.
[47] P.C. Ke, S. Lin, W.J. Parak, T.P. Davis, F. Caruso, A Decade of the protein corona, ACS Nano 11 (2017) 11773–11776.
[48] O. Vilanova, J.J. Mittag, P.M. Kelly, S. Milani, K.A. Dawson, J.O. Rädler, G. Franzese, Understanding the kinetics of protein–nanoparticle corona formation, ACS Nano 10 (2016) 10842–10850.
[49] R. Frost, C. Langhammer, T. Cedervall, Real-time in situ analysis of biocorona formation and evolution on silica nanoparticles in defined and complex biological environments, Nanoscale 9 (2017) 3620–3628.
[50] J.N. Belling, J.A. Jackman, S. Yorulmaz Avsar, J.H. Park, Y. Wang, M.G. Potroz, A.R. Ferhan, P.S. Weiss, N.-J. Cho, Stealth immune properties of graphene oxide enabled by surface-bound complement factor H, ACS Nano 10 (2016) 10161–10172.
[51] F. Chen, G. Wang, J.I. Griffin, B. Brenneman, N.K. Banda, V.M. Holers, D.S. Backos, L. Wu, S.M. Moghimi, D. Simberg, Complement proteins bind to nanoparticle protein corona and undergo dynamic exchange in vivo, Nat. Nanotechnol. 12 (2017) 387–393.
[52] S.M. Moghimi, A.C. Hunter, Complement monitoring of carbon nanotubes, Nat. Nanotechnol. 5 (2010) 382 -382.
[53] A.A. Vertegel, R.W. Siegel, J.S. Dordick, Silica nanoparticle size influences the structure and enzymatic activity of adsorbed lysozyme, Langmuir 20 (2004) 6800–6807.
[54] B. Bharti, J. Meissner, G.H. Findenegg, Aggregation of silica nanoparticles directed by adsorption of lysozyme, Langmuir 27 (2011) 9823–9833.
[55] E.A. Vogler, Protein adsorption in three dimensions, Biomaterials 33 (2012) 1201–1237.
[56] A.J. Clark, A. Kotlicki, C.A. Haynes, L.A. Whitehead, A New model of protein adsorption kinetics derived from simultaneous measurement of mass loading and changes in surface energy, Langmuir 23 (2007) 5591–5600.
[57] J.J. Gray, The interaction of proteins with solid surfaces, Curr. Opin. Struct. Biol. 14 (2004) 110–115.
[58] A.R. Ferhan, J.A. Jackman, N.-J. Cho, Integration of quartz crystal microbalance-dissipation and reflection-mode localized surface plasmon resonance sensors for biomacromolecular interaction analysis, Anal. Chem. 88 (2016) 12524–12531.
[59] E.M. Larsson, M.E.M. Edvardsson, C. Langhammer, I. Zorić, B. Kasemo, A combined nanoplasmonic and electrodeless quartz crystal microbalance setup, Rev. Sci. Instrum 80 (2009) 125105.
[60] D. Campoccia, L. Montanaro, C.R. Arciola, A review of the biomaterials technologies for infection-resistant surfaces, Biomaterials 34 (2013) 8533–8554.
[61] Z. Li, J.C. Barnes, A. Bosoy, J.F. Stoddart, J.I. Zink, Mesoporous silica nanoparticles in biomedical applications, Chem. Soc. Rev. 41 (2012) 2590–2605.
[62] S.A. Ragland, A.K. Criss, From bacterial killing to immune modulation: recent insights into the functions of lysozyme, PLOS Pathog 13 (2017) e1006512.
[63] A.S. Parmar, M. Muschol, Hydration and hydrodynamic interactions of lysozyme: effects of chaotropic versus kosmotropic Ions, Biophys. J. 97 (2009) 590–598.
[64] A.J. Haes, S. Zou, G.C. Schatz, R.P. Van Duyne, Nanoscale optical biosensor: short range distance dependence of the localized surface plasmon resonance of noble metal nanoparticles, J. Phys. Chem. B 108 (2004) 6961–6968.
[65] A.V. Whitney, J.W. Elam, S. Zou, A.V. Zinovev, P.C. Stair, G.C. Schatz, R.P. Van Duyne, Localized surface plasmon resonance nanosensor: a high-resolution distance-dependence study using atomic layer deposition, J. Phys. Chem. B 109 (2005) 20522–20528.
[66] K. Xu, M.M. Ouberai, M.E. Welland, A comprehensive study of lysozyme adsorption using dual polarization interferometry and quartz crystal microbalance with dissipation, Biomaterials 34 (2013) 1461–1470.
[67] M. Aramesh, O. Shimoni, K. Ostrikov, S. Prawer, J. Cervenka, Surface charge effects in protein adsorption on nanodiamonds, Nanoscale 7 (2015) 5726–5736.
[68] J. Meissner, A. Prause, B. Bharti, G.H. Findenegg, Characterization of protein adsorption onto silica nanoparticles: influence of pH and ionic strength, Colloid Polym. Sci. 293 (2015) 3381–3391.

[69] G. Yu, J. Zhou, Understanding the curvature effect of silica nanoparticles on lysozyme adsorption orientation and conformation: a mesoscopic coarse–grained simulation study, Phys. Chem. Chem. Phys. 18 (2016) 23500–23507.
[70] X. Sun, Z. Feng, L. Zhang, T. Hou, Y. Li, The selective interaction between silica nanoparticles and enzymes from molecular dynamics simulations, PLOS ONE 9 (2014) e107696.
[71] B. Masschalck, C.W. Michiels, Antimicrobial properties of lysozyme in relation to foodborne vegetative bacteria, Crit. Rev. Microbiol. 29 (2003) 191–214.
[72] Y. Ye, S. Klimchuk, M. Shang, J. Niu, Improved antibacterial performance using hydrogel-immobilized lysozyme as a catalyst in water, RSC Adv. 9 (2019) 20169–20173.
[73] N.E. Gibbons, C. Winder, E. Barron, D. Fernandes, J.M. Krysmann, A. Kelarakis, V.S.A. Parry, G.S. Yeates, Layer by layer antimicrobial coatings based on nafion, lysozyme, and chitosan, Nanomaterials 9 (2019) 1563.
[74] K.M. Mayer, J.H. Hafner, Localized surface plasmon resonance sensors, Chem. Rev. 111 (2011) 3828–3857.
[75] J.N. Anker, W.P. Hall, O. Lyandres, N.C. Shah, J. Zhao, R.P. Van Duyne, Biosensing with plasmonic nanosensors, Nat. Mater. 7 (2008) 442–453.
[76] K.A. Willets, R.P. Van Duyne, Localized surface plasmon resonance spectroscopy and sensing, Annu. Rev. Phys. Chem. 58 (2007) 267–297.
[77] S.H. Kristensen, G.A. Pedersen, L.N. Nejsum, D.S. Sutherland, Protein adsorption at nanopatterned surfaces studied by quartz crystal microbalance with dissipation and surface plasmon resonance, J. Phys. Chem. B 117 (2013) 10376–10383.
[78] J.H. Park, T.N. Sut, J.A. Jackman, A.R. Ferhan, B.K. Yoon, N.-J. Cho, Controlling adsorption and passivation properties of bovine serum albumin on silica surfaces by ionic strength modulation and cross-linking, Phys. Chem. Chem. Phys. 19 (2017) 8854–8865.
[79] J.H. Park, A.R. Ferhan, J.A. Jackman, N.-J. Cho, Modulating conformational stability of human serum albumin and implications for surface passivation applications, Colloids Surf. B Biointerfaces 180 (2019) 306–312.
[80] P.M. Biesheuvel, M. van der Veen, W. Norde, A modified Poisson−Boltzmann model including charge regulation for the adsorption of ionizable polyelectrolytes to charged interfaces, applied to lysozyme adsorption on silica, J. Phys. Chem. B 109 (2005) 4172–4180.
[81] K. Kubiak-Ossowska, M. Cwieka, A. Kaczynska, B. Jachimska, P.A. Mulheran, Lysozyme adsorption at a silica surface using simulation and experiment: effects of pH on protein layer structure, Phys. Chem. Chem. Phys. 17 (2015) 24070–24077.
[82] M. Lundin, U.M. Elofsson, E. Blomberg, M.W. Rutland, adsorption of lysozyme, β-casein and their layer-by-layer formation on hydrophilic surfaces: effect of ionic strength, Colloids Surf. B Biointerfaces 77 (2010) 1–11.
[83] T. Nezu, T. Masuyama, K. Sasaki, S. Saitoh, M. Taira, Y. Araki, Effect of pH and addition of salt on the adsorption behavior of lysozyme on gold, silica, and titania surfaces observed by quartz crystal microbalance with dissipation monitoring, Dent. Mater. J. 27 (2008) 573–580.
[84] M. van der Veen, W. Norde, M.C. Stuart, Electrostatic interactions in protein adsorption probed by comparing lysozyme and succinylated lysozyme, Colloids Surf. B Biointerfaces 35 (2004) 33–40.
[85] J. Buijs, V. Hlady, Adsorption kinetics, conformation, and mobility of the growth hormone and lysozyme on solid surfaces, studied with TIRF, J. Colloid Interface Sci 190 (1997) 171–181.
[86] M.J. Penna, M. Mijajlovic, M.J. Biggs, Molecular-level understanding of protein adsorption at the interface between water and a strongly interacting uncharged solid surface, J. Am. Chem. Soc. 136 (2014) 5323–5331.
[87] K. Kubiak-Ossowska, P.A. Mulheran, Mechanism of hen egg white lysozyme adsorption on a charged solid surface, Langmuir 26 (2010) 15954–15965.
[88] M. Tang, N.S. Gandhi, K. Burrage, Y. Gu, Adsorption of collagen-like peptides onto gold nanosurfaces, Langmuir 35 (2019) 4435–4444.
[89] C. Zhang, X. Li, Z. Wang, X. Huang, Z. Ge, B. Hu, Influence of structured water layers on protein adsorption process: a case study of cytochrome c and carbon nanotube interactions and its implications, J. Phys. Chem. B 124 (2020) 684–694.